

MoErv29 promotes apoplasmic effector secretion contributing to virulence of the rice blast fungus *Magnaporthe oryzae*

Bin Qian^{1,2,3}, Xiaotong Su^{1,2,3}, Ziyuan Ye^{1,2,3}, Xinyu Liu^{1,2,3}, Muxing Liu^{1,2,3}, Danyu Shen^{1,2}, Han Chen^{1,2}, Haifeng Zhang^{1,2,3} , Ping Wang⁴ and Zhengguang Zhang^{1,2,3} 

¹Department of Plant Pathology, College of Plant Protection, Nanjing Agricultural University, Nanjing 210095, China; ²Key Laboratory of Integrated Management of Crop Diseases and Pests, Ministry of Education, Nanjing 210095, China; ³The Key Laboratory of Plant Immunity, Nanjing Agricultural University, Nanjing 210095, China; ⁴Department of Microbiology, Immunology and Parasitology, Louisiana State University Health Sciences Center, New Orleans, LA 70118, USA

Summary

Author for correspondence:
Zhengguang Zhang
Email: zhgzhang@njau.edu.cn

Received: 4 August 2021
Accepted: 1 November 2021

New Phytologist (2022) 233: 1289–1302
doi: 10.1111/nph.17851

Key words: cytoplasmic coat protein complex II (COPII), effector secretion, *Magnaporthe oryzae*, pathogenicity, unfolded protein response (UPR).

- During plant-pathogenic fungi and host plants interactions, numerous pathogen-derived proteins are secreted resulting in the activation of the unfolded protein response (UPR) pathway. For efficient trafficking of secretory proteins, including those important in disease progression, the cytoplasmic coat protein complex II (COPII) exhibits a multifunctional role whose elucidation remains limited.
- Here, we discovered that the COPII cargo receptor MoErv29 functions as a target of MoHac1, a previously identified transcription factor of the UPR pathway. In *Magnaporthe oryzae*, deletion of *MoERV29* severely affected the vegetative growth, conidiation and biotrophic invasion of the fungus in susceptible rice hosts.
- We demonstrated that MoErv29 is required for the delivery of secreted proteins through recognition and binding of the amino-terminal tripeptide motifs following the signal peptide. By using bioinformatics analysis, we predicted a cargo spectrum of MoErv29 and found that MoErv29 is required for the secretion of many proteins, including extracellular laccases and apoplasmic effectors. This secretion is mediated through the conventional endoplasmic reticulum–Golgi secretion pathway and is important for conferring host recognition and disease resistance.
- Taken together, our results revealed how MoErv29 operates on effector secretion, and our findings provided a critical link between COPII vesicle trafficking and the UPR pathway.

Introduction

In eukaryotic cells, endoplasmic reticulum (ER) is the major intracellular organelle responsible for protein synthesis (Tabas & Ron, 2011). During the development of various human and plant-pathogenic fungi, the concerted upregulation of effector gene expression has resulted in a dramatically increased influx of nascent proteins into the ER, causing ER stress that triggers the unfolded protein response (UPR). This counter-response is critical for ER stress resistance and the virulence of the fungi (Walter & Ron, 2011; Askew, 2014; Krishnan & Askew, 2014). In *Aspergillus fumigatus*, the ER transmembrane stress sensor IreA synergises with the canonical UPR, independent of the HacA transcription factor, to influence virulence traits (Feng *et al.*, 2011). In *Cryptococcus neoformans*, UPR functions in parallel with the calcineurin and MAPK signalling pathways to evade the human immune system (Cheon *et al.*, 2011). The *Ustilago maydis* UPR is related to the regulation of biotrophic development and timely induction following plant penetration. In addition, the UPR regulator Cib1 interacts with the developmental regulator Clp1 that leads to the accumulation of Clp1 protein and triggers re-initiation of mitotic growth *in planta* (Heimel *et al.*, 2013).

Moreover, a higher ER stress is induced during the biotrophic phase of the hemibiotrophic fungus *Magnaporthe oryzae* that causes rice blast (Tang *et al.*, 2015; Yin *et al.*, 2020). Various studies have shown that most secreted and transmembrane proteins are synthesised, folded, and matured at ER, including a third of newly synthesised misfolded proteins that induce ER stress (Ron & Walter, 2007). To counteract this, cells activate the UPR pathway to degrade these misfolded proteins (Hwang & Qi, 2018). In *M. oryzae*, the UPR pathway transcription activator MoHac1 is alternatively spliced to regulate the expression of several putative target genes involved in ER stress responses, including a nucleotide exchange factor (*MoSIL1*), chaperone dnaJ 2 (*MoSCJ1*), ER-derived vesicles protein (*MoERV29*), translocation of misfolded proteins out of ER (*MoSEC61*), protein disulfide isomerase1 (*MoPDII*), ER protein chaperone BiP (*MoKAR2*), and ER-associated degradation (*MoDER1*) (Travers *et al.*, 2000; Tang *et al.*, 2015). This indicated that the UPR activity would lead to the alteration of the secretory pathway that also affects effector secretion.

Once synthesised in the ER, proteins are transported to the Golgi for further maturation (Ron & Walter, 2007; Brandizzi & Barlowe, 2013). However, the diffusion of cargo proteins from

the ER lumen into cargo vesicles destined to the Golgi apparatus ('bulk flow') is insufficient. Cargo receptors have long been proposed to bind specific cargo proteins in coat protein complex II (COPII) exit vesicles for more efficient ER trafficking. Examination of the purified COPII vesicles revealed a group of ER vesicle (Erv) proteins that function as cargo receptors to recognise and efficiently pack specific cargos into the vesicles (Otte & Barlowe, 2002). These Erv proteins show various molecular masses and are mostly transmembrane proteins (Otte & Barlowe, 2002; Herzig *et al.*, 2012). Among them, Surf4, a homologue of the yeast Erv29 found in human embryonic kidney cell line 293A (HEK293A), differentially binds to tripeptide motifs, enabling prioritisation of their exit from the ER that is also important for the triggering of the UPR pathway (Yin *et al.*, 2018).

In *M. oryzae*, effector secretion follows two distinct patterns of accumulation within the extra-invasive hyphal membrane (EIHM) compartment enclosing invasive hyphae (IH) (Giraldo *et al.*, 2013). Apoplastically secreted effectors are dispersed within the EIHM compartment and do not enter host cells, whereas cytoplasmic effectors mostly accumulate in the biotrophic interfacial complex (BIC), a membrane-rich structure that initially appears adjacent to primary hyphal tips, but is later positioned subapically as IH develop within rice cells (Giraldo *et al.*, 2013; Zhang & Xu, 2014). Although other fungal studies have suggested a connection between the UPR and general secretory pathway, the detailed links between UPR and COPII-mediated protein secretion is unclear, and the mechanism of how UPR regulates effector secretion remains unknown in *M. oryzae*.

Here, we identified MoErv29 as a target of the UPR pathway regulated by MoHac1 and showed that MoErv29 is involved in regulating the growth, conidiation and virulence of *M. oryzae*. In addition, we provided evidence demonstrating that MoErv29 is required for the delivery of secreted proteins, and this requirement is made possible through the recognition of amino-terminal tripeptide motifs. Moreover, we identified a putative cargo spectrum of MoErv29 through bioinformatics analysis, substantiating that MoErv29 is involved in the secretion of extracellular proteins such as laccases and effectors. Taken together, our studies established a new connection between COPII vesicle trafficking and UPR signalling and provided novel insights into how effector proteins may be secreted and regulated during infection.

Materials and Methods

Strains and culture conditions

Magnaporthe oryzae Guy11 was used as the wild-type strain in this research. All strains were cultured on a complete medium (CM) at 28°C. For vegetative growth, small blocks were cut from the edge of 7-d-old cultures and placed onto fresh medium, followed by incubation in the dark at 28°C. Radial growth was then measured after incubation for 7 d. Other media, including oatmeal agar medium (OM) and minimal medium (MM), were prepared as described previously (Qian *et al.*, 2018). Liquid CM was used to prepare the vegetative mycelia for DNA and RNA

extraction. For conidiation, mycelial blocks were inoculated onto straw decoction and corn agar medium (SDC) (100 g of rice straw decoction was boiled in 1 l of ddH₂O for 20 min and filtered, and the filtrate was mixed with 40 g of cornmeal and 15 g of agar and adjusted to 1 l with ddH₂O) at 28°C for 7 d in the dark and followed by 3 d of continuous illumination under fluorescent light (Qi *et al.*, 2016).

In vivo co-immunoprecipitation assay

The empty green fluorescent protein (GFP) construct was obtained in our previous work (Qian *et al.*, 2020). The *MoSLP1* DNA fragment fused with the S tag was inserted into the pXY203 construct (*MoSLP1-S*) containing the hygromycin resistance, and the *MoERV29* DNA fragment fused with GFP (*MoERV29-GFP*) was inserted into the pYF11 construct containing the bleomycin (R25001; Thermo Fisher Scientific, Waltham, MA, USA) resistance gene. Then *MoSLP1-S/MoERV29-GFP* and *MoSLP1-S/GFP* constructs were co-transformed into wild-type strain Guy11, and transformants resistant to hygromycin and bleomycin were isolated. Total proteins were extracted from the transformants using protein lysis buffer (50 mM Tris-HCl, pH 7.4, with 150 mM NaCl, 1 mM EDTA, and 1% Triton X-100 (T8787; Sigma-Aldrich) and incubated with anti-S agarose for 4 h, followed by washing the affinity gel with Tris-buffered saline (TBS) (50 mM Tris-HCl, 150 mM NaCl, pH 7.4) four times. The proteins bound to the affinity gel were eluted with 0.1 M glycine HCl (pH 2.5) and were detected by anti-S and anti-GFP antibodies (Abmart, Shanghai, China).

Electrophoretic mobility shift assay

The DNA fragment from the *MoERV29* promoter was end-labelled with Alex660 by polymerase chain reaction (PCR) amplification using the 5' Alex660-labelled primer. The purified MoHac1^S protein was mixed with Alex660-labelled DNA, incubated for 20 min at 25°C in binding buffer (45 mM Tris, 45 mM boric acid, pH 8.4), and separated by electrophoresis in 1% agarose with 0.5 TBE (45 mM Tris, 45 mM boric acid, 1 mM EDTA, pH 8.0) agarose gel electrophoresis. Gels were directly visualised using an LI-COR Odyssey scanner with excitation at 700 nm.

MoERV29 gene deletion and complementation

The Δ *Moerv29* mutants were generated using a one-step gene replacement strategy. Two fragments with 1.0 kb of sequences flanking the targeted gene were PCR amplified with primer pairs (Supporting Information Table S1). The resulting PCR products were ligated to the hygromycin (H8080; Solarbio® Life Sciences, Beijing, China) resistance cassette (*HPH*) released from pCX62. The 3.4-kb fragment, which included the flanking sequences and the *HPH* cassette, was transformed into Guy11 protoplasts. Putative mutants were screened by PCR and confirmed using Southern blot analysis. For complementation, the fragment containing the entire *MoERV29* gene coding region and its native promoter

region was amplified using PCR with primers (Table S1) before insertion into pYF11 and introduced into the mutant strain. Other gene deletion mutants and corresponding complemented strains were obtained using the same strategy (Qian *et al.*, 2020).

Construction of the Δ Mohac1, Δ Mohac1/MoHAC1^{mut intron}, Δ Mohac1/MoHAC1^S, and Δ Mohac1/MoHAC1 strains

The Δ Mohac1, Δ Mohac1/MoHAC1^{mut intron}, Δ Mohac1/MoHAC1^S, and Δ Mohac1/MoHAC1 strains had been obtained in the laboratory previously (Tang *et al.*, 2015). Δ Mohac1/MoHAC1^{mut intron} represents the mutant carrying several site-directed mutations in the unconventional intron that was unable to process splicing of the unconventional intron and Δ Mohac1/MoHAC1^S represents the mutant lacking the unconventional intron. The mutation sites are shown in Fig. S1. The generation strategy has been described previously in Tang *et al.* (2015).

Assays for pathogenicity and penetration

Pathogenicity tests were carried out in detached rice and barley seedling leaves using the mycelia of Guy11, the Δ Moerv29 mutant, and the complemented strain. For the mutants of MoErv29 cargo proteins, conidia were collected from 10-d-old SDC agar cultures and resuspended using 0.2% (w/v) gelatin (G8061; Solarbio) solution to a concentration of 5×10^4 spores ml⁻¹. For the spraying assay, 2-wk-old rice seedlings (*Oryza sativa* cv CO-39) were sprayed with 4 ml of a conidial suspension of each treatment and kept in a growth chamber at 25°C with 90% humidity in the dark for the first 24 h, followed by a 12 h : 12 h, light : dark cycle. Lesion formation was daily checked and photographed after 7 d of inoculation (Li *et al.*, 2019). The 7-d-old barley leaves were drop-inoculated with three droplets (20 μ l) of conidial suspension, and photographs were taken 5 d after infection. Each experiment was repeated more than three times, and the experimental conditions were controlled to be consistent (e.g. temperature, humidity, illumination and the age of the plants). For the 'relative fungal growth' assay, total DNA was extracted from 1.5 g disease leaves and tested using quantitative real-time PCR (qRT-PCR) with 28S/Rubq1 primers (Table S1) (Zhong *et al.*, 2016). For rice sheath penetration and IH expansion, the conidial suspension (1×10^5 spores ml⁻¹) was inoculated into the sheaths. After incubation for 36 h at 28°C, the sheath cuticle cells were observed under a Zeiss Axio Observer A1 inverted microscope (Li *et al.*, 2017).

Quantitative RT-PCR analysis

For detection of *MoSLP1* expression, constructs of *MoSLP1*^{APP}, *MoSLP1*^{IPV}, and *MoSLP1*^{EET} were transformed into the Δ Moslpl1 and Δ Moerv29 mutants. RNA was extracted from the mycelia and reverse transcribed into cDNA using the HiScript II cDNA synthesis kit (R233-01; Vazyme Biotech Co., Nanjing, China). Transcript detection of target genes was measured, and the transcription of the *ACTIN* gene (XP_003719871.1) was used as

endogenous control. qRT-PCR was run on the Applied Biosystems 7500 Real-Time PCR System with SYBR Premix Ex Taq (Perfect Real-Time, Takara, Japan).

To detect rice pathogenesis-related (PR) gene transcription during the invasion growth stage, total RNA was extracted from plants inoculated with the mycelium of wild-type strain or mutant after 24 and 48 hours post-inoculation (hpi). Transcription of the host *ACTIN* gene (XM_015774830.2) was used as the endogenous control. The primer design was similar to that previously reported (Wang *et al.*, 2013). qRT-PCR was run on the Applied Biosystems 7500 Real-Time PCR System using the ChamQ SYBR[®] qPCR Master Mix (Q311-02/03; Vazyme Biotech Co.).

Reactive oxygen species observation

To observe reactive oxygen species (ROS) derived from the host, barley leaves or rice sheaths were stained with 3,3'-diaminobenzidine (DAB) (Sigma-Aldrich). Barley leaves inoculated with the mutant and wild-type strains for 24 hpi were incubated in 1 mg ml⁻¹ DAB solution, pH 3.8, at room temperature for 8 h and destained with clearing solution (ethanol : acetic acid, 94 : 4, v/v) for 1 h. The back epidermises of infected cells were harvested and observed under a microscope (Liu *et al.*, 2018). For luminol chemiluminescence assay (Liu *et al.*, 2019), rice protoplasts were prepared, or leaves were cut into discs with a cork borer and preincubated overnight in sterile-distilled water in a 96-well plate. The water was replaced with luminol (35.4 μ g ml⁻¹), and peroxidase (10 μ g ml⁻¹) solution and 50 nM purified mycelia (PRM) were used as the elicitor (Liu *et al.*, 2019). Luminescence was measured using a GLOMAX96 microplate luminometer (Promega, Madison, WI, USA).

Results

Identification of MoErv29 as a target of MoHac1

To explore how effector proteins are secreted via vesicle trafficking and its regulation in the ER stress response and virulence of the blast fungus, we focused on the previously characterised transcription factor MoHac1 and its putative targets. As MoErv29 is a homologue of the yeast Erv29p, MoErv29 could partially rescue the growth defect of the yeast Δ Scerv29 mutant upon dithiothreitol (DTT)-induced stress (Fig. S2) and as a previous study had shown that Erv29p was upregulated under ER stress (Yin *et al.*, 2020), we selected MoErv29 for further characterisation.

We first verified whether *MoERV29* was a target gene of MoHac1. qRT-PCR showed that *MoERV29* was highly expressed under DTT-induced ER stress in the wild-type strain Guy11, but not in the Δ Mohac1 mutant or the Δ Mohac1/MoHac1^{mut intron} strain. In addition, overexpression of *MoERV29* could be partially induced in the Δ Mohac1/MoHac1^S strain independent of DTT treatment (Fig. 1a). To further understand the regulation between MoHac1 and *MoERV29*, we used the electrophoretic mobility shift assay to verify that MoHac1 indeed bound to the promoter region of *MoERV29*. This binding was

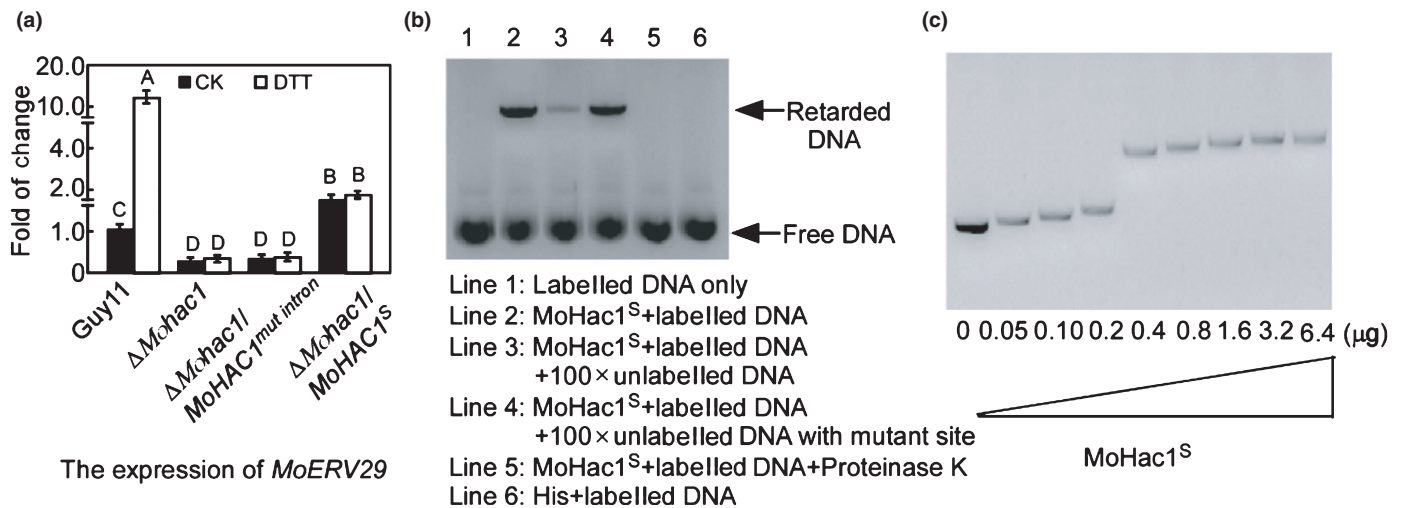


Fig. 1 Electrophoretic mobility shift assay of MoHac1 binding to the promoter of *MoERV29*. (a) Expression analysis of *MoERV29* in the Δ MoHac1 mutant and wild-type strains with or without dithiothreitol treatment, Δ MoHac1/MoHAC1^{mut intron} represents the nonspliced MoHac1, and Δ MoHac1^S represents the spliced MoHac1. Error bars represent \pm SD and different letters represent significant differences ($P < 0.01$). CK, ddH₂O control. (b) Alex660-labelled *MoERV29* promoter (80 nmol) was incubated in the absence (lane 1) or the presence of purified MoHac1^S (0.4 μ g) (lane 2) and competed with 100× unlabelled *MoERV29* promoter (lane 3). Lane 4: Labelled *MoERV29* promoter competed with 100× unlabelled *MoERV29* promoter in which the MoHac1 binding site (CACGT) was deleted. Lane 5: Proteinase K was added after the incubation of MoHac1^S with the *MoERV29* promoter. Lane 6: Labelled *MoERV29* promoter was incubated with empty His. The DNA-protein complexes were separated by electrophoresis on a 1% agarose gel. (c) Alex660-labelled *MoERV29* promoter 1500 bp (5 nmol) was incubated with the MoHac1^S protein (μ g) in a concentration gradient, and the complexes were resolved by electrophoresis on a 1% agarose gel.

diminished when proteinase K was added or when the binding motif (CACGT), predicated by JASPAR (<http://jaspar.genereg.net/>), was mutated (Fig. 1b). Moreover, the band for the *MoERV29* DNA promoter (5 nmol) migrated gradually with the increased amount of purified MoHac1 protein, and this retardation reached saturation when $> 0.4 \mu$ g MoHac1 was added (Fig. 1c). The above result, therefore, indicated that *MoERV29* is a target of MoHac1 involved in the ER stress response.

MoErV29 is important for vegetative growth, conidiation and infection

To examine MoErV29 function in *M. oryzae*, we generated Δ Moerv29 mutants and verified their genotypes using PCR, Southern blot and qRT-PCR analysis (Fig. S3a–d). The Δ Moerv29 mutants showed no significant reduction in vegetative growth compared with Guy11 and the complemented Δ Moerv29/*MoERV29* strain on CM, MM, SDC, and OM media (Fig. 2a,b). However, colonies formed by the Δ Moerv29 mutants were much thinner than with Guy11 and the complemented strains following a 7 d incubation on CM (Fig. 2c). We also found that the Δ Moerv29 mutants could not produce conidia on SDC medium (Fig. 2d,e). These results indicated that MoErV29 was required for airborne hyphal growth and asexual development of *M. oryzae*.

Due to *MoERV29* being highly expressed during infection (Fig. S4), we explored the role of MoErV29 in pathogenicity. As the Δ Moerv29 mutants could not produce conidia, the mycelia of Guy11, the Δ Moerv29 mutant, and the complemented strain were used to inoculate detached rice and barley seedling leaves.

The Δ Moerv29 mutant caused very restricted lesions on unwounded leaves compared with Guy11 and the complementation Δ Moerv29/*MoERV29* strain (Fig. 3a). On wounded barley leaves, the Δ Moerv29 mutant produced limited lesions (Fig. 3b), and a similar result was also observed on infected rice leaves (Fig. 3c,d).

As the Δ Moerv29 mutant caused limited lesions, we speculated that MoErV29 might have a role in regulating IH growth. In a barley penetration assay, the Δ Moerv29 mutant showed 15% type 1, 25% type 2, 43% type 3, and 17% type 4 infectious hyphal growth, in comparison with which there was *c.* 5% type 1, 10% type 2, 25% type 3, and 60% type 4 infectious hyphal growth for Guy11 and the complemented Δ Moerv29/*MoERV29* strain (Fig. 3e,f). Therefore, we concluded that MoErV29 was important for vegetative growth, conidiation and IH growth of *M. oryzae*.

MoErV29 is involved in the scavenging of reactive oxygen species

Host ROS generation acts as a defensive mechanism against fungal IH growth (Guo *et al.*, 2011; Liu *et al.*, 2020). Based on the restricted lesions caused by the Δ Moerv29 mutant being similar to the resistant-type lesions, we examined whether MoErV29 was involved in ROS scavenging by measuring ROS production in barley cells using DAB staining at 24 hpi (Chen *et al.*, 2014). Of the barley cells infected with the Δ Moerv29 mutant, 65% were stained brown, compared with 13% and 15% of those infected with Guy11 and the complemented strain, respectively (Fig. 4a, b). We assumed that limited IH growth and decreased virulence

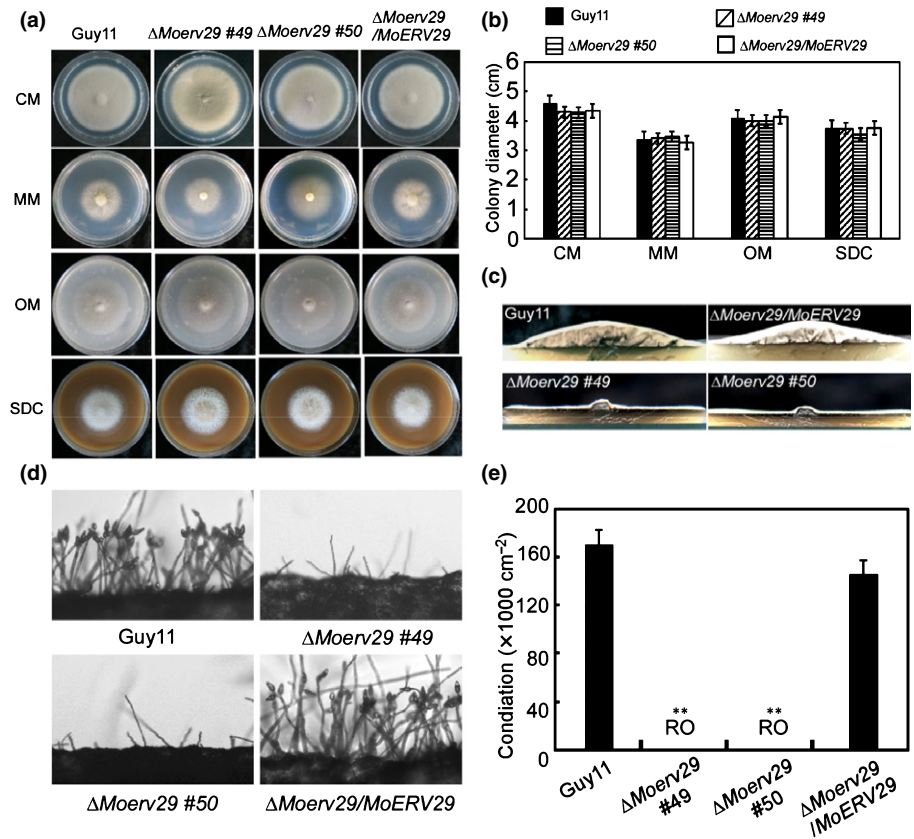


Fig. 2 MoErV29 is required for vegetative growth and conidiation. (a) Guy11, $\Delta Moerv29$ mutants, and $\Delta Moerv29/MoERV29$ were inoculated on complete medium, minimal medium, oatmeal agar medium, and straw decoction and corn agar medium and incubated at 28°C for 7 d before being photographed. (b) Statistical analysis of the colony diameter of indicated strains. Error bars represent \pm SD. (c) The $\Delta Moerv29$ mutant appears as a flat colony with thin aerial hyphal growth when compared with the wild-type Guy11. (d) Conidia were observed under a light microscope after illumination for 24 h and photographed. (e) Statistical analysis of conidial numbers of the indicated strains. Error bars represent \pm SD. **, $P < 0.01$. RO, rarely observed.

might be caused by a defect in the $\Delta Moerv29$ mutant to scavenge host ROS. We, therefore, used diphenyleneiodonium (DPI) to inhibit the nicotinamide adenine dinucleotide phosphate (NADPH) oxidase activity (Liu *et al.*, 2021) necessary for host ROS generation and found that, when treated with 0.5 μM DPI, certain $\Delta Moerv29$ IH could spread into neighbouring cells (Fig. 4c,d). These observations suggested that MoErV29 was involved in scavenging ROS and the virulence defect of the $\Delta Moerv29$ mutant may be partly due to the accumulation of host ROS.

ROS is also a diffusible second messenger for defence signalling and defence gene induction (Nurnberger *et al.*, 2004; Huang *et al.*, 2011). To further investigate whether plant defence genes were activated in infection by the $\Delta Moerv29$ mutant, we detected the transcript levels of four rice defence-related genes involved in salicylic acid (SA) (*PRIa*, *Chl1*, and *PAL1*) and jasmonic acid (JA) (*PBZ1* and *AOS2*) pathways using qRT-PCR (Qian *et al.*, 2018; Zhang *et al.*, 2019). The transcript levels of these genes were much higher in infection by the $\Delta Moerv29$ mutant than that by Guy11 at 24 and 48 hpi (Fig. 4e,f). Taken together, we proposed that the limited IH of the $\Delta Moerv29$ mutant might be due to the accumulation of host-derived ROS that triggers a defensive response in the host.

The subcellular localisation of MoErV29 in *M. oryzae*

To reveal how MoErV29 orchestrated virulence, we first examined the spatial and temporal distribution of MoErV29. We

obtained a $\Delta Moerv29/MoERV29-GFP$ strain in which the expression of the C-terminal fused GFP was under the control of the native *MoERV29* promoter. We found that MoErV29-GFP could be localised to morphologically distinct and highly dynamic vesicular membrane structures. We also found that this localisation was co-localised with FM4-64-stained vesicles within the growing hyphal tips (Fig. 5a). To further determine if MoErV29-labelled vesicles could be co-localised with the ER or Golgi, we used the RFP-tagged MoLhs1 and MoSft2 proteins that are markers of the ER and Golgi, respectively (Yi *et al.*, 2009; Zhang *et al.*, 2017). Indeed, MoErV29-GFP could be partially co-localised with MoLhs1 and MoSft2 (Fig. 5b). As COPII vesicle trafficking is a dynamic process from the ER to the Golgi and MoErV29 is a COPII cargo receptor, we monitored by live-cell time-lapse imaging whether MoErV29 was dynamically involved in the transport. As brefeldin A (BFA) inhibits protein transport from the ER to the Golgi by preventing the association of COPII coat proteins with the Golgi, we used BFA and found that MoErV29 function could be inhibited by BFA (Fig. 5c). Moreover, when we compared the intracellular distribution of MoErV29-GFP at the ER and Golgi apparatus with or without the BFA treatment, the results showed that without treatment *c.* 70% MoErV29 was co-located with the Golgi and 30% MoErV29 was co-located with the ER. However, when treated with BFA, nearly 80% MoErV29 was co-located with the ER, and only 20% MoErV29 was co-located with the Golgi (Fig. S5a–c). The above results suggested that MoErV29 is important for ER-to-Golgi traffic.

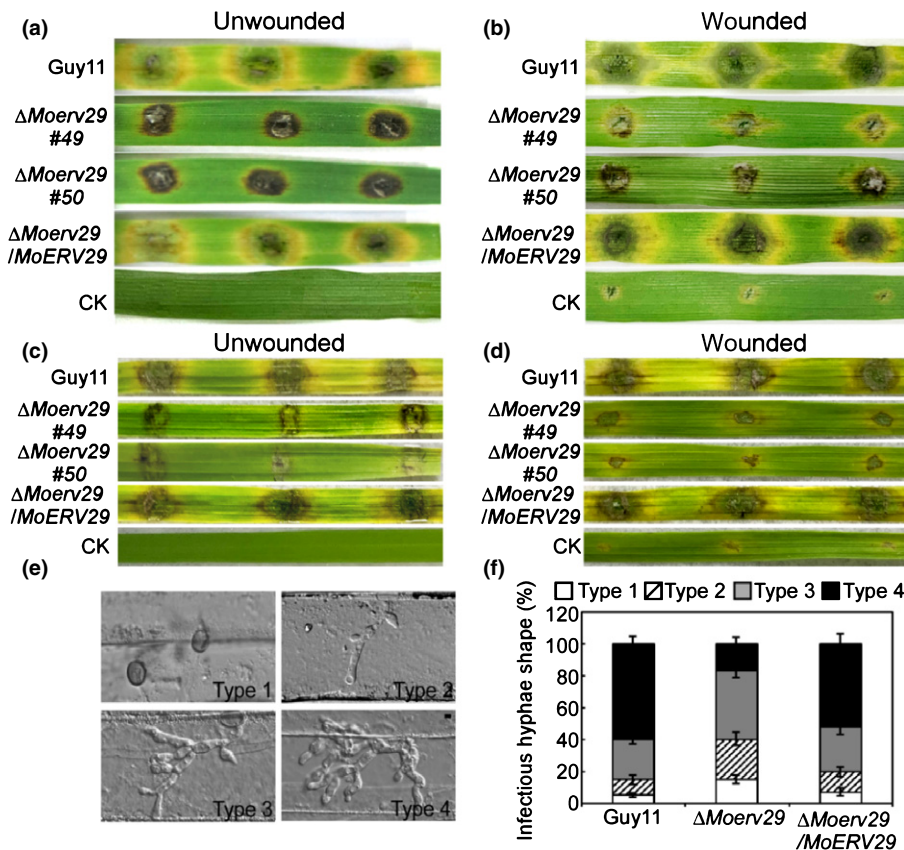


Fig. 3 MoErV29 is required for pathogenicity. (a) Pathogenicity test on unwounded and detached barley leaves. Photographs were taken at 7 d. CK, ddH₂O control. (b) Detached barley leaves wounded by abrasion and inoculated with the mycelia of Guy11, $\Delta Moerv29$ mutants, and complemented strains. Photographs of wounded leaves at 5 d after inoculation. (c, d) Pathogenicity test on rice. Detached rice leaves were inoculated with the mycelia of Guy11, $\Delta Moerv29$ mutants, and complemented strains. Unwounded leaves were photographed at 7 d and wounded leaves 5 d after inoculation. (e, f) Statistical analysis for each type of infectious hyphal shape. Type 1, no penetration; type 2, only with a single invasive hypha without branches; type 3, with 1–3 branches but restricted in one cell; type 4, more than three branches and extended to the neighbouring cell. For each tested strain, 100 infecting hyphae ($n = 100$) were counted per replicate, and the experiment was repeated three times with similar results. (e) Bar, 10 μ m. (f) Error bars represent \pm SDs.

MoErV29 interacts with and is involved in the secretion of the apoplastic effector MoSlp1

Magnaporthe oryzae has two types of effector secretion systems, the cytoplasmic effectors that are accumulated in the BIC and the apoplastic effectors that are retained within the EIHM compartment (Giraldo *et al.*, 2013). Previous studies have demonstrated that *M. oryzae* interferes with host immunity during infection by secreting various effector proteins to scavenge host-derived ROS (Dong *et al.*, 2015; Zhang *et al.*, 2016). The function of MoErV29 in ER-to-Golgi trafficking and the strong immunity triggered by the $\Delta Moerv29$ mutant suggested that the $\Delta Moerv29$ mutant could be impaired in effector secretion. We introduced AvrPiz-t and AvrPia into Guy11 and the $\Delta Moerv29$ mutant to evaluate their subcellular localisation. Cells infected by Guy11 showed nearly 90% of effectors in the BIC, in contrast with cells infected with the $\Delta Moerv29$ mutant for which no difference was found (Fig. S6). However, the apoplastic effector MoSlp1 was found within the EIHM compartment in Guy11 but not the $\Delta Moerv29$ mutant in which GFP fluorescence was diffused into the cytoplasm (Fig. 6a). This diffused MoSlp1-GFP distribution was similar to that in wild-type cells treated with BFA (Fig. 6b). These results suggested that MoErV29 was involved in the secretion of apoplastic effectors, including MoSlp1.

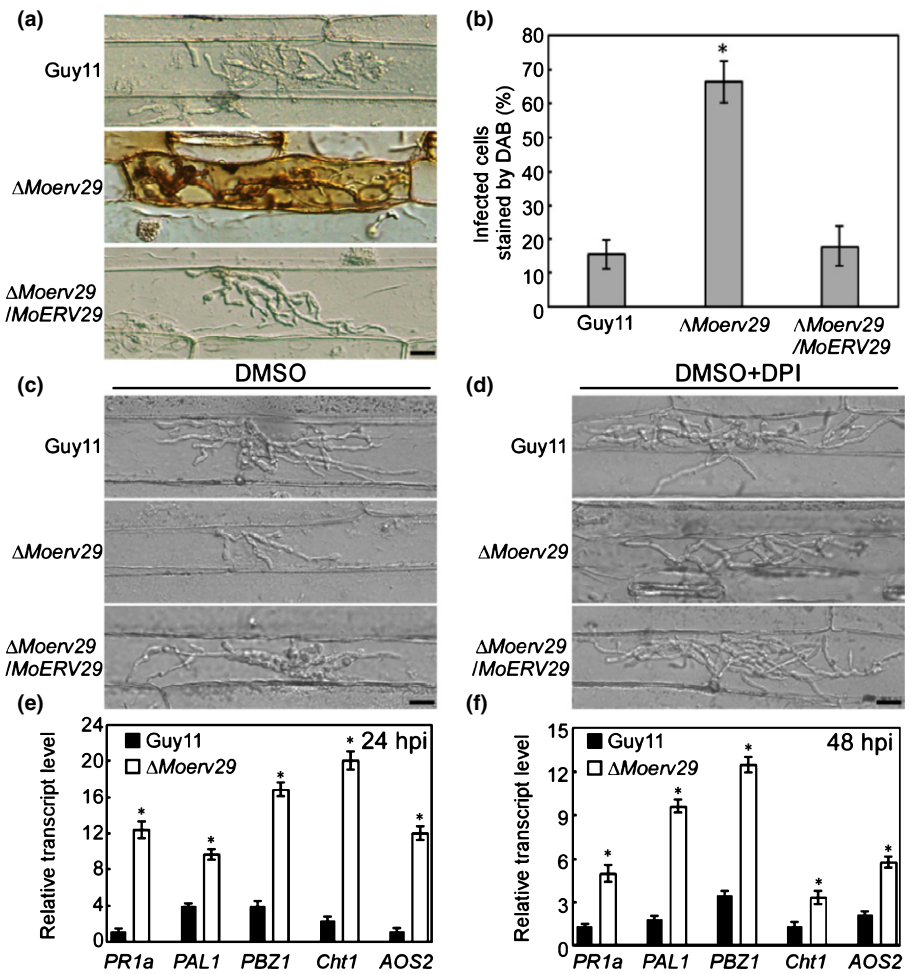
A previous study identified three *N*-glycosylation sites and three forms of MoSlp1 (MoSlp1-1, MoSlp1-2, and MoSlp1-3) in *M. oryzae* that were essential for its stability (Chen *et al.*,

2014). To test whether the diffused cytoplasmic distribution of MoSlp1 in the $\Delta Moerv29$ mutant affected this *N*-glycosylation, we fused MoSlp1 with an S tag and introduced it into Guy11 and the $\Delta Moerv29$ mutant strains. Total proteins were extracted from Guy11/*MoSLP1-S* and $\Delta Moerv29$ /*MoSLP1-S* strains and subjected to immunoblot analysis with an anti-S antibody. All these forms of MoSlp1 were detected in Guy11 and the $\Delta Moerv29$ mutant. However, a significant accumulation in protein levels was observed for MoSlp1-1, MoSlp1-2, or MoSlp1-3 in the $\Delta Moerv29$ mutant in comparison with the wild-type Guy11 strain (Fig. 6c). In addition, a co-immunoprecipitation (Co-IP) assay showed that MoErV29 interacted with MoSlp1 (Fig. 6d). These results indicated that MoErV29 was required for the efficient secretion of MoSlp1.

MoErV29 binds to the amino-terminal tripeptide motifs of MoSlp1

As MoErV29 is involved in the secretion of MoSlp1, we further explored the probable recognition mechanism of MoSlp1 by MoErV29. Previous studies have indicated that the human Surf4 protein preferred to bind to the amino-terminal tripeptide motif following the signal peptide with a varied affinity that prioritises its exit from the ER (Yin *et al.*, 2018). The tripeptide motif is normally comprised of hydrophobic–proline–hydrophobic amino acids of soluble cargo proteins (after removal of the signal peptide sequences). A match in all three positions enables high-affinity

Fig. 4 MoErV29 is important for suppressing the production of host reactive oxygen species (ROS). (a) 3,3'-Diaminobenzidine (DAB) staining on infected barley cells of CO39 with Guy11, Δ Moerv29 mutants, and the complement strains at 24 h post-inoculation (hpi). Bar, 10 μ m. (b) Graphics represents the percentage of the invaded barley cells ($n = 100$) stained by DAB. Error bars represent \pm SD; *, $P < 0.01$. (c, d) Diphenyleneiodonium (DPI) treatment was used to inhibit the activity of nicotinamide adenine dinucleotide phosphate oxidases, which are necessary generators of plant ROS. Dimethyl sulphoxide treatment was a control that is used to dissolve DPI. Bar, 10 μ m. (e, f) Expression analysis of defence-related genes by quantitative real-time PCR at 24 and 48 hpi. The average threshold cycle of triplicate reactions was normalised to elongation factor 1a (*EF1a*, Os03g08020) in *O. sativa*. Three independent biological experiments were performed and yielded similar results. Error bars represent \pm SD; asterisks represent significant differences (*, $P < 0.01$).



binding, while a modest affinity is found if two positions match and low-affinity if one position matches (Yin *et al.*, 2018).

To test whether the MoSlp1 recognition by MoErV29 used a similar mechanism, the approaches of site-directed mutagenesis and *in vivo* transformation were used to generate mutant versions of MoSlp1. We replaced the MoSlp1 native tripeptide motif glycine–proline–proline (APP) with two mutant motifs: isoleucine–proline–valine (IPV) strong binding motif and glutamic acid–glutamic acid–threonine (EET) nonbinding motif. Western blot analysis showed that the *MoSLP1-S* in Δ *Moslp1* with IPV and APP motifs was rarely detected, and the EET motif exhibited a significant accumulation similar to that in the Δ *Moerv29* mutant (Fig. 7a). Also, qRT-PCR analysis revealed that the expression of *MoSLP1* was not different among the six tested strains (Fig. 7b). Then, we detected the secretion of MoSlp1-GFP fusion proteins with different tripeptide motifs. In the complementation strains that had the APP native motif or were changed to have the IPV motif, MoSlp1 was found in the EIHM structure. However, when replaced with the nonbinding EET motif, MoSLP1^{EET} was retained in the ER and co-localised with the ER marker MoLhs1 (Fig. 7c). In the Δ *Moerv29* mutant, the subcellular localisation of MoSlp1 showed no difference among IPV, APP, and EET motifs (Fig. 7d). Also, the Co-IP assay showed that the IPV motif had a higher binding affinity

than the native APP motif and the EET nonbinding motif (Fig. 7e). Moreover, we found that the *MoSLP1*^{IPV} construct could complement the virulence of Δ *Moslp1* more efficiently than *MoSLP1*^{EET} (Fig. 7f).

Finally, when observing the secretion of another apoplastic effector, MoBas4, that contains the nonbinding amino-terminal tripeptide motifs, there was no difference between Guy11 and the Δ *Moerv29* mutant as MoBas4-GFP was located in the EIHM of both strains (Fig. S7). Taken together, these results suggested that MoErV29 binds to amino-terminal tripeptide motifs of soluble cargo proteins in some way when being exported out of the ER.

Identification of putative cargo spectrum of MoErV29 with tripeptide motifs and characterisation of MoErV29 in regulating extracellular protein activities

As we had verified that MoErV29 binds with amino-terminal tripeptide motifs of cargo proteins, we sought to systematically identify all putative cargo proteins that contained at least one position match for *M. oryzae*. In total, 1010 proteins were identified from the Fungidb (Fungi DB, 2021) database (Table S2). To validate the function of cargo proteins, we performed Gene Ontology of all 1010 proteins (Table S3). As shown in Fig. S8, MoErV29 was closely involved in the

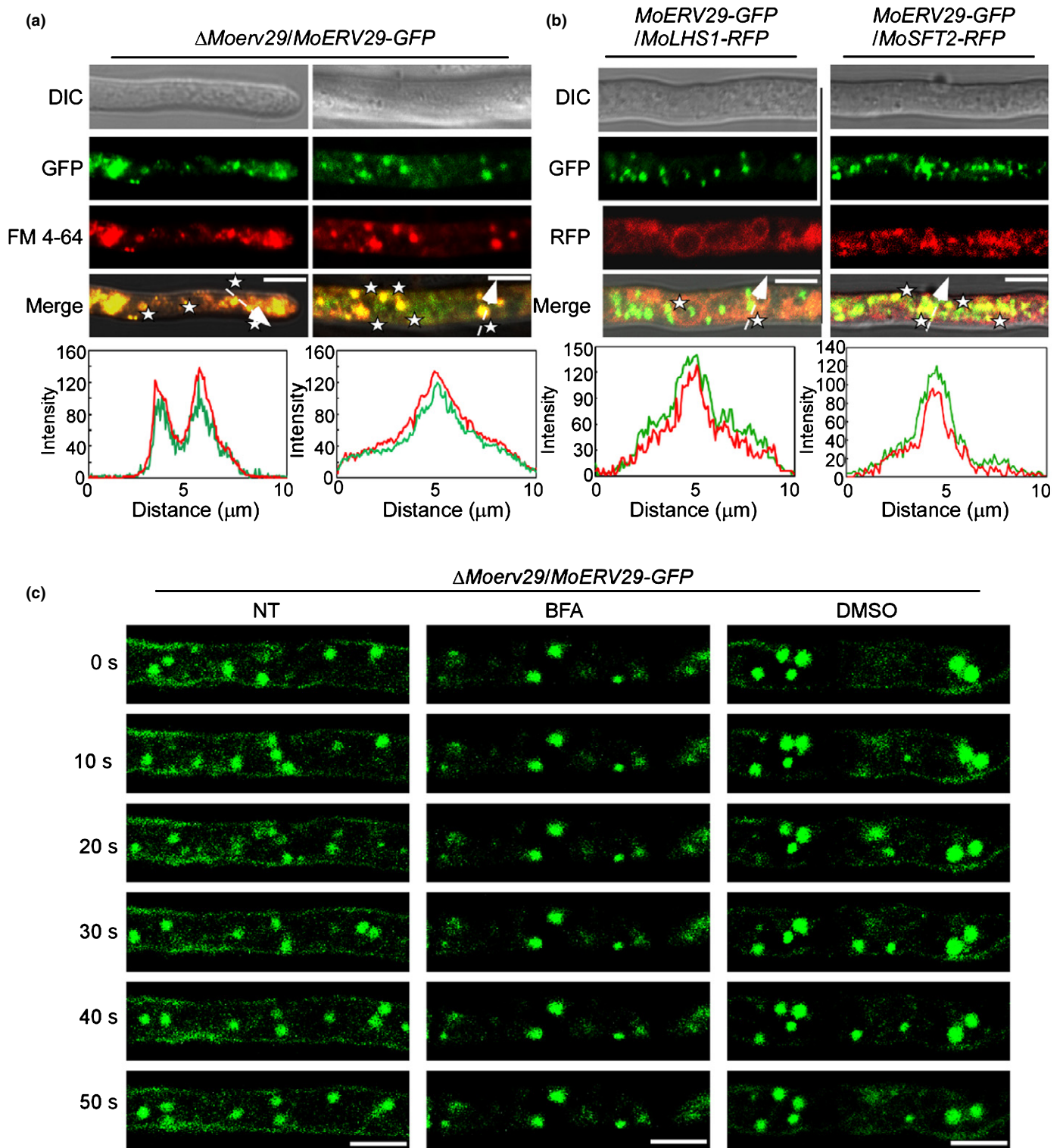


Fig. 5 Subcellular localisation of MoErV29 in *Magnaporthe oryzae*. (a) Hyphae of transformants that expressed *MoERV29-GFP* were observed under a confocal microscope ($\times 63$ oil; Zeiss LSM710). The cells were stained with FM4-64 for 3 min. Bar, 10 μm . Line-scan graph analysis showed that MoErV29-GFP was co-localised with FM4-64-stained vesicles. White asterisks indicate merged vesicles. (b) The localisation pattern of MoErV29 with the ER and Golgi marker, respectively. Fluorescence images were captured using a confocal microscope ($\times 63$ oil; Zeiss LSM710), and line-scan graph analysis indicated that MoErV29-GFP was partially co-localised with ER and Golgi. Bar, 10 μm . White asterisks indicate merged vesicles. (c) Time-lapse images of cells expressing the *MoERV29-GFP* reporter at different time intervals with or without treatment of ER–Golgi protein trafficking inhibitor brefeldin A. Dimethyl sulphoxide was used as a control. The white arrow with dotted line indicates the areas used for linescan graph analysis. NT, no treatment. Bar, 10 μm .

Fig. 6 MoErv29 interacts with and is involved in the secretion of apoplast effector MoSlp1. (a) The subcellular location of MoSlp1-GFP was observed in barley cells incubated with Guy11 or the Δ Moerv29 mutant. Photographs were taken at 24 h post-inoculation (hpi). Bar, 10 μ m. (b) Subcellular location of MoSLP1-GFP was observed when treated with brefeldin A (BFA) or dimethyl sulphoxide (DMSO). DMSO was used as a control, as DMSO was used to dissolve BFA. Bar, 10 μ m. (c) Western blot assays for N-glycosylation of MoSlp1 in the wild-type and the Δ Moerv29 mutant strains. Total proteins were isolated from the separated transformants of Guy11/MoSLP1-S and Δ Moerv29/MoSLP1-S and detected with an anti-S antibody. (d) Co-immunoprecipitation assay shows that MoErv29-GFP interacts with MoSlp1-S. The empty green fluorescent protein construct was used as a control.

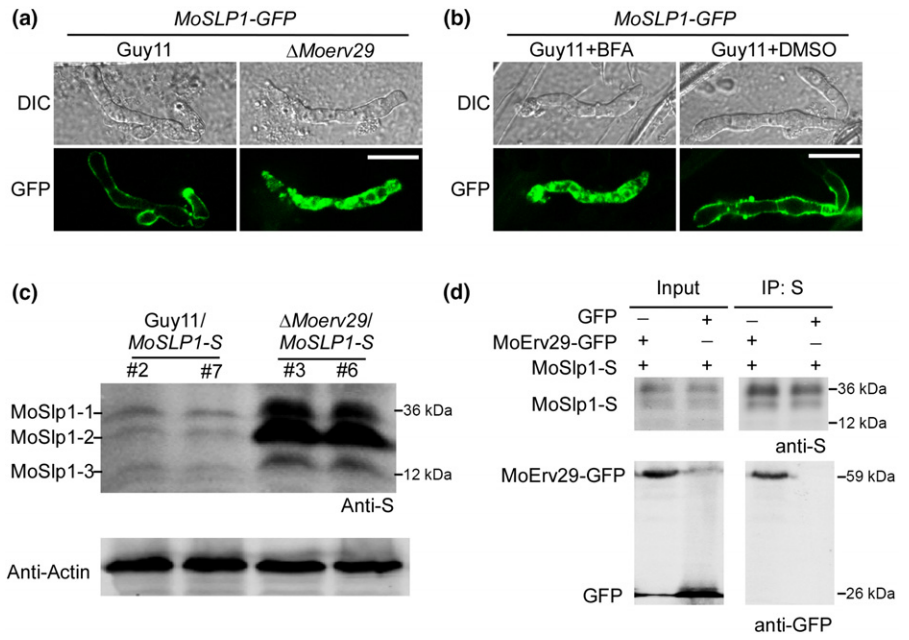
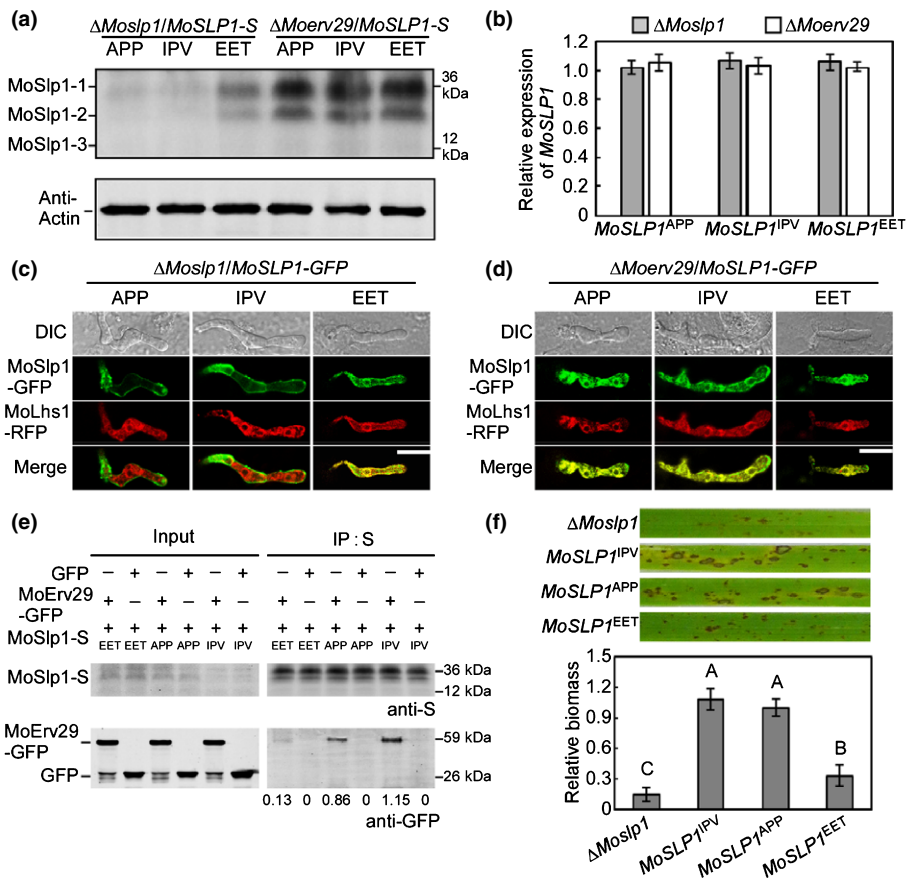


Fig. 7 MoErv29 binds to the amino-terminal tripeptide motifs of MoSlp1. (a) N-glycosylation of MoSlp1 was detected using western blot analysis in the Δ Moslp1 and the Δ Moerv29 with native amino-terminal tripeptide motifs, high-affinity motif (IPV), and nonbinding motif (EET) after the removal of the signal peptide. (b) Expression of MoSLP1 with different variants in Δ Moslp1 and Δ Moerv29. Error bars represent \pm SD. (c, d) Subcellular localisation of MoSlp1 variant in Δ Moslp1 and Δ Moerv29. MoLhs1 was used as an endoplasmic reticulum track marker. Bar, 10 μ m. (e) The binding affinities of MoErv29 with different tripeptide motifs in *Magnaporthe oryzae*, the empty green fluorescent protein construct was used as a control. (f) Conidial suspensions of the Δ Moslp1 mutant and MoSlp1 variant were suspended to a concentration of 5×10^4 spores ml^{-1} and sprayed onto 2-wk-old rice seedlings, photographed at 7 days post-inoculation (dpi). The severity of blast disease was evaluated by quantifying *M. oryzae* genomic 28S rDNA relative to rice genomic Rubq1 DNA. The mean values of three determinations with SD are shown. Analysis of variance was used for the statistical analysis; different letters indicate a significant difference ($P < 0.01$).



secretion of extracellular proteins such as peroxidases, laccases and chitinases. To validate the involvement of MoErv29 in the secretion of peroxidases and laccases, we monitored their activities using Congo red and 2,2'-azino-di-3-ethylbenzthiazoline-6-

sulfonate (ABTS). Discoloured halos were observed surrounding the colonies of Guy11 but not the Δ Moerv29 mutant (Fig. S9a,b). Also, a decreased laccase activity was seen in the Δ Moerv29 mutant, with nearly no visible oxidised dark purple

stain around its colony. Further colorimetric assays revealed severely impaired peroxidase and laccase activities in the culture filtrate of the $\Delta Moerv29$ mutant compared with the wild-type Guy11 strain (Fig. S9c,d). Considered together, the above results indicated the importance of MoErV29 in virulence by regulating the secretion of extracellular redox enzymes.

MoErV29 regulates the secretion of a novel EIHM subcellular protein MoEcp1

To further test if cargo proteins of MoErV29 had a role in ROS detoxification and virulence, we examined the expression profiles of the cargo proteins for those with an increased expression during infection and randomly observed the subcellular localisation of nine selected proteins (Fig. S10). Interestingly, all nine selected proteins exhibited an EIHM subcellular localisation in Guy11 but cytoplasmic retention in the $\Delta Moerv29$ mutant (Fig. 8a). We further generated deletion mutants for these nine genes and found that the $\Delta Moecp1$ mutant (MoEcp1, MGG_00259, a MoErV29 Cargo Protein 1) was significantly attenuated in

virulence. All other eight mutants were dispensable for pathogenicity (Fig. 8b,c).

We then investigated whether the secretion and pathogenicity of MoEcp1 depended on the tripeptide motif. As shown in Fig. 9 (a,b), when the tripeptide motif was altered to the low-affinity EET motif, MoEcp1 was retained in the ER rather than secreted into the EIHM, and its virulence was also reduced (Fig. 9c,d). Also, ROS was rarely detected in infection sites by $MoECPI^{IPV}$ and $MoECPI^{APV}$ ($< 10\%$, $n = 50$). In comparison, high ROS levels were observed in cells infected by the $\Delta Moecp1$ mutant and $MoECPI^{EET}$ ($> 60\%$, $n = 50$) (Fig. 9e). Using a luminol-based chemiluminescence assay (Alfano & Collmer, 2004; Ghosh, 2004; Liu *et al.*, 2019, 2021), we observed that the *in vitro* expression of MoEcp1 could suppress the flg22-triggered increase in ROS (Fig. 9f).

To study the role of MoErV29 in effector secretion precisely, the cytoplasmic effector AvrPi9 that contains the high-affinity amino-terminal tripeptide motif was fused with GFP and transformed into Guy11 and the $\Delta Moerv29$ mutant. However, the AvrPi9-GFP was secreted into BIC in both Guy11 and the

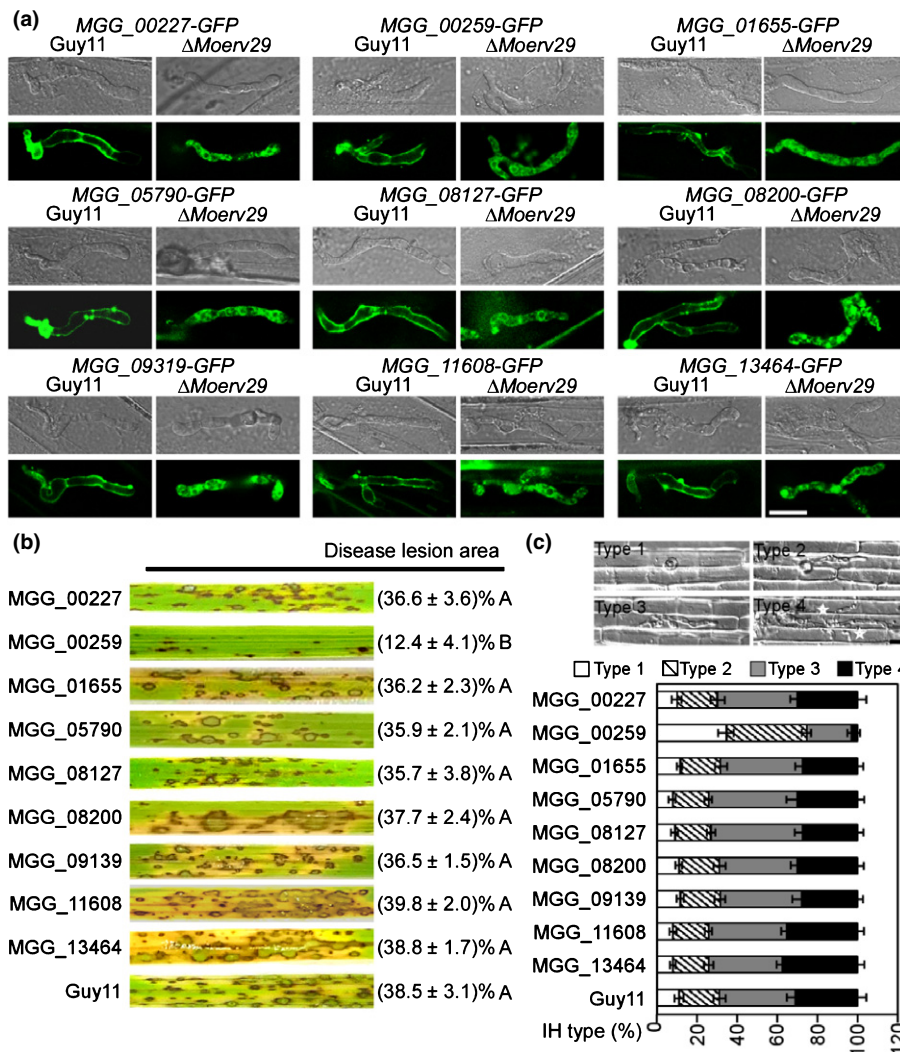


Fig. 8 The subcellular localisation and virulence assay of nine putative cargo proteins of MoErV29. (a) Nine putative cargo proteins of MoErV29 were selected, fused with the green fluorescent protein tag, and then introduced into Guy11 and $\Delta Moerv29$ for subcellular localisation observation. Bar, 10 μ m. (b) For the virulence assay, conidial suspensions of Guy11 and the nine selected gene mutants were suspended to a concentration of 5×10^4 spores ml^{-1} and sprayed onto 2-wk-old rice seedlings. Diseased rice leaves were photographed at 7 days post-inoculation (dpi). The disease lesion area (%) was assessed using IMAGEJ software. There were three replicates each of 10 leaves. Analysis of variance was used for statistical analysis, and different letters indicate significant differences ($P < 0.01$). (c) For observation of the penetration and invasive growth in rice cells, conidial suspensions (1×10^5 spores ml^{-1}) were injected into the rice leaf sheath. At 28°C for 30 h, the infected sheaths were observed under a microscope. The percentage of a pattern showed in the image was calculated by observation for 50 penetration sites, and the observation was repeated three times, error bars represent \pm SDs. Bar, 10 μ m.

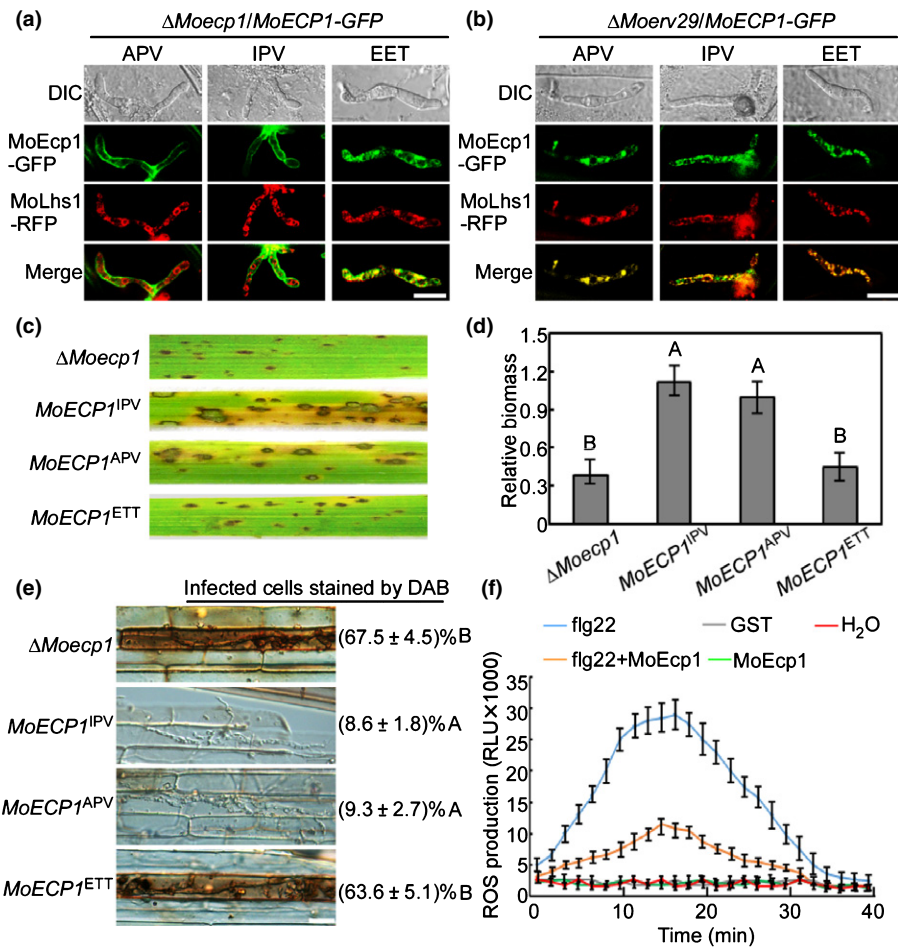


Fig. 9 MoErV29 regulates the secretion of MoEcp1, an extra-invasive hyphal membrane subcellular protein important for reactive oxygen species (ROS) detoxification. (a, b) The native tripeptide motifs (APV) of MoEcp1 in the amino-terminal following the removal of the peptide sequence changed with the high-affinity motif isoleucine–proline–valine (IPV) and the nonbinding motif glutamic acid–glutamic acid–threonine (EET), fused with green fluorescent protein (GFP), and then observed for localisation in $\Delta Moecp1$ and $\Delta Moerv29$ mutants. Bar, 10 μ m. (c) Conidial suspensions of strains $\Delta Moecp1$, MoEcp1 with high-affinity motifs ($MoECP1^{IPV}$), MoEcp1 with native tripeptide motifs ($MoECP1^{APV}$), and MoEcp1 with nonbinding motifs ($MoECP1^{ETT}$) were suspended to a concentration of 5×10^4 spores ml^{-1} and sprayed onto 2-wk-old rice seedlings. Diseased rice leaves were photographed at 7 days post-inoculation (dpi). (d) The severity of blast disease was evaluated by quantifying *Magnaporthe oryzae* genomic 28S rDNA relative to rice genomic Rubq1 DNA. The mean values of three determinations with SD are shown. Analysis of variance (ANOVA) was used for the statistical analysis; different letters indicate a significant difference ($P < 0.01$). (e) 3,3'-Diaminobenzidine (DAB) staining on infected rice sheath of CO39 at 24 h post-inoculation (hpi) with $\Delta Moecp1$, $MoECP1^{IPV}$, $MoECP1^{APV}$ and $MoECP1^{ETT}$ complemented strains. The percentages donate the infected cells stained by DAB ANOVA was used for the statistical analysis, and different letters indicated a significant difference. Bar, 10 μ m. (f) MoEcp1 inhibits ROS burst in the CO39 rice plant. Rice protoplast from CO39 was treated with purified MoSef1 protein, 100 nM flg22, glutathione S-transferase (GST) or water and ROS were detected with a luminol-chemiluminescent assay. Error bars represent the SD ($n = 3$).

$\Delta Moerv29$ mutant (Fig. S11). These studies further demonstrated that MoErV29 regulates the secretion of apoplastic effectors, including MoEcp1, to play an important role in ROS detoxification and pathogenicity.

Discussion

For successful colonisation, phytopathogenic pathogens secrete large numbers of effector proteins to manipulate host immunity (Fernandez & Orth, 2018). It is well known that bacterial plant pathogens secrete effector proteins via type III and type IV secretion systems (Alfano & Collmer, 2004; Ghosh, 2004). In fungal phytopathogens, effector secretion is beginning to be explored. In

M. oryzae, previous studies have revealed two distinctive effector secretion systems. The first is that cytoplasmic effectors destined for delivery inside rice cells are secreted by a BFA-insensitive pathway involving the exocytosis complex. The second is that apoplastic effectors are secreted via a conventional ER-to-Golgi secretory process that is sensitive to BFA inhibition (Giraldo *et al.*, 2013). Previous studies also identified the exocyst components and SNARE proteins as the docking subunits tethering vesicles to the secretory sites (Khang *et al.*, 2010; Heider & Munson, 2012). Also, studies found that the Qc-SNARE protein MoSyn8 is required for the secretion of cytoplasmic effectors Avr-Pia and AvrPiz-t but not apoplastic effectors (Qi *et al.*, 2016). In addition, the endocytic protein MoEnd3 was required

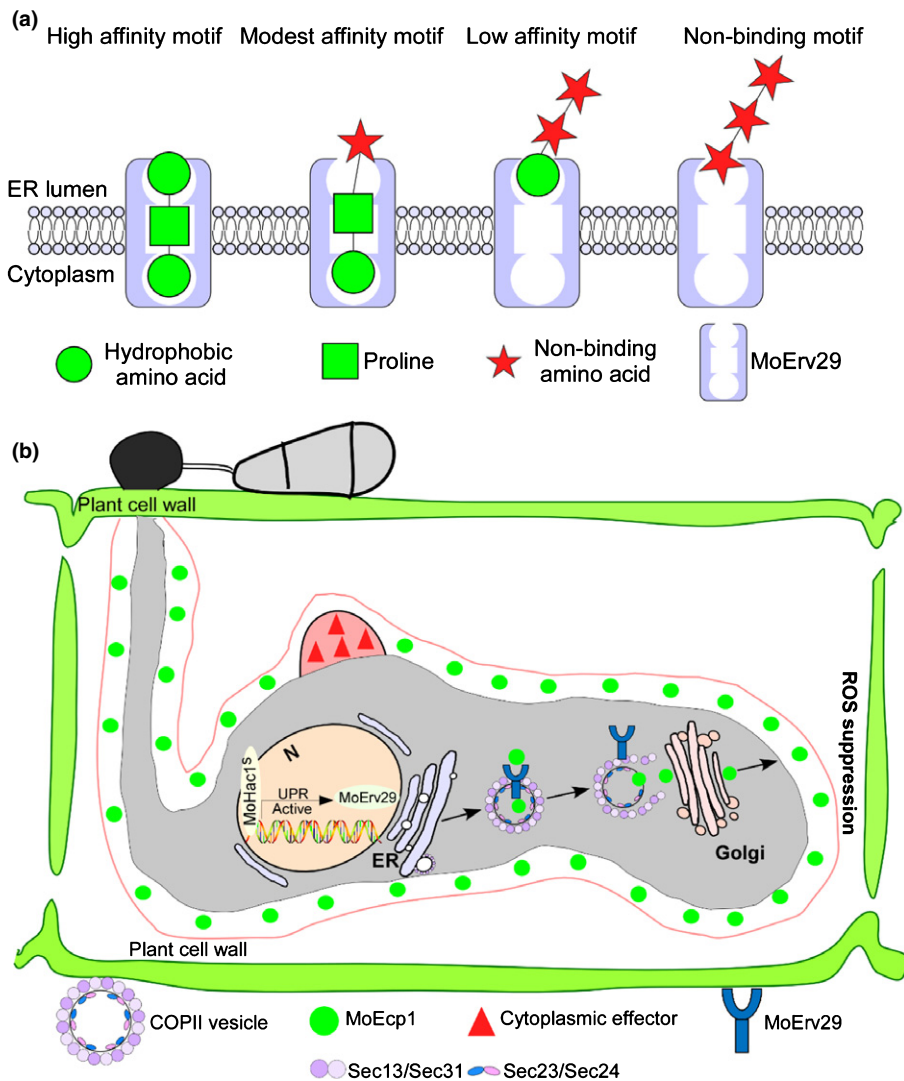


Fig. 10 A working model of the MoEr29-mediated secretion pathway in *Magnaporthe oryzae*. (a) MoEr29 functions as a coat protein complex II (COPII) cargo receptor that binds to the amino-terminal tripeptide motifs of effector proteins (after removal of signal peptide sequences) with different affinities, enabling prioritisation of their exit from the endoplasmic reticulum (ER). The optimal contribution of that residue to binding affinity was a proline in the number 2 position and a hydrophobic residue in positions 1 (amino terminus) and 3. High-affinity occurred when matches were found in all three positions, while modest affinity was found when two positions matched, and low-affinity was found when only one position matched. (b) During infection, *M. oryzae* secretes large numbers of effector proteins to manipulate plant immunity. The apoplastic effectors are secreted through a conventional process via the ER-to-Golgi pathway. Here, MoEr29 functions as a COPII cargo receptor that binds to the amino-terminal tripeptide motifs of effector proteins with different affinities. The secreted process is regulated by the unfolded protein response (UPR) pathway transcription activator MoHac1 that controls the expression level of MoEr29. ROS, reactive oxygen species.

for the secretion of cytoplasmic effectors Avr-Pia and AvrPiz-t, but not AvrPib and AvrPi9 (Li *et al.*, 2017). These results indicated that while vesicle trafficking is important for effector secretion during infection, the secretion of different effectors depended on distinct vesicle transport pathways. Given that MoEr29 is involved in the COPII-dependent vesicle trafficking of apoplastic effectors and is dispensable for cytoplasmic effectors Avr-Pia and AvrPiz-t secretion, it is plausible that COPII-mediated trafficking is important for apoplastic effector secretion. The latest study revealed that MoSwa2 mediated the secretion of both cytoplasmic and apoplastic proteins to govern the pathogenicity of *M. oryzae* (Liu *et al.*, 2021). How these effectors are sorted into distinct vesicles remains unclear.

Cytoplasmic coat protein complex II cargo receptors have long been proposed to bind specific cargo proteins in COPII exit vesicles for more efficient ER trafficking (Belden & Barlowe, 2001; Herzig *et al.*, 2012; Yin *et al.*, 2018). In *S. cerevisiae*, the best known cargo proteins of Erv29p were the vacuole carboxypeptidase Y (CPY, PRC1) and mating factor alpha-1 ($mf\alpha$ -1, MAT1) (Belden & Barlowe, 2001; Otte & Barlowe, 2004). *S. cerevisiae* $mf\alpha$ -1 has three *N*-linked oligosaccharides spaced along its

64-aminoacid prepro-domain and successive or combinatorial loss of these modifications and deletions within the domain of amino acids 23–37 or 29–63 all resulted in significant, but incomplete, loss of hormone secretion (Caplan *et al.*, 1991). Using a series of alanine substitutions, previous studies have found that three large hydrophobic amino acids (I39, L42, and V52) constituted the prepro motif that binds to Erv29p (Otte & Barlowe, 2004). In addition, when changes were made in this motif (L42S and V52A), pro- $mf\alpha$ -1 exhibited an increased secretion rate (Rakestraw *et al.*, 2009). So, it remains unclear how I39, L42, and V52 exhibit the change in the trafficking of pro- $mf\alpha$ -1.

Yin *et al.* (2018) proposed that yeast Erv29 establishes different steady-state concentrations for a variety of soluble cargo proteins within the ER through interactions with the amino-terminal tripeptides exposed after the removal of leader sequences. We here also propose that the mechanism by which MoEr29 promotes the apoplastic effector secretion is based on the ER transport (Fig. 10). Based on the tripeptide motifs of MoEr29, we predicted its cargo spectrum and verified the prediction that MoEr29 is involved in the secretion of peroxidases, laccases and certain specific cargo effectors. We demonstrated that all of the

cargo effectors containing the binding motif to MoErv29 were mis-localised in the $\Delta Moeru29$ mutants. This finding may suggest that the motif could be used in the identification of new apoplastic effectors. In addition, as certain apoplastic effectors, such as Bas4 that lacks the amino-terminal tripeptide motifs for binding, are still localised at the EIHM, COPII-mediated apoplastic effector secretion may also be regulated differently.

To conclude, we demonstrated a new effector protein secretion strategy of *M. oryzae* in which the receptor-enhanced ER trafficking of secreted proteins with tripeptide motifs followed a conserved fashion, and we propose that the apoplastic effectors may use this secretion strategy during infection of the blast fungus.



Acknowledgements

This research was supported by the programme of NSFC-DFG (grant no. 31861133017), the China National Funds for Innovative Research Groups (grant no. 31721004), NSFC (31772110), and the Youth Program for Natural Science Foundation of Jiangsu Province (BK20200543). Research in the PW laboratory was supported by award AI156254 from NIH (USA).

Author contributions

BQ and ZZ designed research; BQ, XS, ZY, XL, ML, DS, HZ and ZZ performed experiments; BQ and ZZ contributed new reagents/analytical tools; BQ, XS, ZY, HC, HZ and XZ analysed data; and BQ, PW and ZZ wrote the manuscript.

ORCID

Haifeng Zhang  <https://orcid.org/0000-0002-7963-9071>
Zhengguang Zhang  <https://orcid.org/0000-0001-8253-4505>

Data availability

The data that support the findings of this study are available in the Supporting Information of this article.

References

- Alfano JR, Collmer A. 2004. Type III secretion system effector proteins: double agents in bacterial disease and plant defense. *Annual Review of Phytopathology* 42: 385–414.
- Askew DS. 2014. Endoplasmic reticulum stress and fungal pathogenesis converge. *Virulence* 5: 331–333.
- Belden WJ, Barlowe C. 2001. Role of Erv29p in collecting soluble secretory proteins into ER-derived transport vesicles. *Science* 294: 1528–1531.
- Brandizzi F, Barlowe C. 2013. Organization of the ER–Golgi interface for membrane traffic control. *Nature Reviews Molecular Cell Biology* 14: 382–392.
- Caplan S, Green R, Rocco J, Kurjan J. 1991. Glycosylation and structure of the yeast MF alpha 1 alpha-factor precursor is important for efficient transport through the secretory pathway. *Journal of Bacteriology* 173: 627–635.
- Chen XL, Shi T, Yang J, Shi W, Gao XS, Chen D, Xu XW, Xu JR, Talbot NJ, Peng YL. 2014. N-Glycosylation of effector proteins by an alpha-1,3-mannosyltransferase is required for the rice blast fungus to evade host innate immunity. *Plant Cell* 26: 1360–1376.
- Cheon SA, Jung KW, Chen YL, Heitman J, Bahn YS, Kang HA. 2011. Unique evolution of the UPR pathway with a novel bZIP transcription factor, Hx11, for controlling pathogenicity of *Cryptococcus neoformans*. *PLoS Pathogens* 7: e1002177.
- Dong Y, Li Y, Zhao M, Jing M, Liu X, Liu M, Guo X, Zhang X, Chen Y, Liu Y *et al.* 2015. Global genome and transcriptome analyses of *Magnaporthe oryzae* epidemic isolate 98–06 uncover novel effectors and pathogenicity-related genes, revealing gene gain and loss dynamics in genome evolution. *PLoS Pathogens* 11: e1004801.
- Feng X, Krishnan K, Richie DL, Aimanianda V, Hartl L, Grahl N, Powers-Fletcher MV, Zhang M, Fuller KK, Nierman WC *et al.* 2011. HacA-independent functions of the ER stress sensor IreA synergize with the canonical UPR to influence virulence traits in *Aspergillus fumigatus*. *PLoS Pathogens* 7: e1002330.
- Fernandez J, Orth K. 2018. Rise of a Cereal Killer: the biology of *Magnaporthe oryzae* biotrophic growth. *Trends in Microbiology* 26: 582–597.
- FungiDB. 2021. *Data set: Pyricularia oryzae 70–15 genome sequence and annotation* [WWW document] URL https://fungidb.org/fungidb/app/record/dataset/DS_d22dd5953a
- Ghosh P. 2004. Process of protein transport by the type III secretion system. *Microbiology and Molecular Biology Reviews* 68: 771–795.
- Giraldo MC, Dagdas YF, Gupta YK, Mentlak TA, Yi M, Martinez-Rocha AL, Saitoh H, Terauchi R, Talbot NJ, Valent B. 2013. Two distinct secretion systems facilitate tissue invasion by the rice blast fungus *Magnaporthe oryzae*. *Nature Communications* 4: 1996.
- Guo M, Chen Y, Du Y, Dong YH, Guo W, Zhai S, Zhang HF, Dong SM, Zhang ZG, Wang YC *et al.* 2011. The bZIP transcription factor MoAP1 mediates the oxidative stress response and is critical for pathogenicity of the rice blast fungus *Magnaporthe oryzae*. *PLoS Pathogens* 7: e1001302.
- Heider MR, Munson M. 2012. Exorcising the exocyst complex. *Traffic* 13: 898–907.
- Heimel K, Freitag J, Hampel M, Ast J, Bolker M, Kamper J. 2013. Crosstalk between the unfolded protein response and pathways that regulate pathogenic development in *Ustilago maydis*. *Plant Cell* 25: 4262–4277.
- Herzig Y, Sharpe HJ, Elbaz Y, Munro S, Schuldiner M. 2012. A systematic approach to pair secretory cargo receptors with their cargo suggests a mechanism for cargo selection by Erv14. *PLoS Biology* 10: e1001329.
- Huang K, Czymmek KJ, Caplan JL, Sweigard JA, Donofrio NM. 2011. HYR1-mediated detoxification of reactive oxygen species is required for full virulence in the rice blast fungus. *PLoS Pathogens* 7: e1001335.
- Hwang J, Qi L. 2018. Quality control in the endoplasmic reticulum: crosstalk between ERAD and UPR pathways. *Trends in Biochemical Sciences* 43: 593–605.
- Khang CH, Berruyer R, Giraldo MC, Kankana P, Park SY, Czymmek K, Kang S, Valent B. 2010. Translocation of *Magnaporthe oryzae* effectors into rice cells and their subsequent cell-to-cell movement. *Plant Cell* 22: 1388–1403.
- Krishnan K, Askew DS. 2014. Endoplasmic reticulum stress and fungal pathogenesis. *Fungal Biology Reviews* 28: 29–35.
- Li X, Gao CY, Li LW, Liu MX, Yin ZY, Zhang HF, Zheng XB, Wang P, Zhang ZG. 2017. MoEnd3 regulates appressorium formation and virulence through mediating endocytosis in rice blast fungus *Magnaporthe oryzae*. *PLoS Pathogens* 13: e1006449.
- Li X, Zhong KL, Yin ZY, Hu JX, Wang WH, Li LW, Zhang HF, Zheng XB, Wang P, Zhang ZG. 2019. The seven transmembrane domain protein MoRgs7 functions in surface perception and undergoes coronin MoCrn1-dependent endocytosis in complex with G subunit MoMagA to promote cAMP signaling and appressorium formation in *Magnaporthe oryzae*. *PLoS Pathogens* 15: e1007382.
- Liu MX, Hu JX, Zhang A, Dai Y, Chen WZ, He YL, Zhang HF, Zheng XB, Zhang ZG. 2021. Auxilin-like protein MoSwa2 promotes effector secretion and virulence as a clathrin uncoating factor in the rice blast fungus *Magnaporthe oryzae*. *New Phytologist* 230: 720–736.
- Liu MX, Zhang SB, Hu JX, Sun WX, Padilla J, He YL, Li Y, Yin ZY, Liu XY, Wang WH *et al.* 2019. Phosphorylation-guarded light-harvesting complex II contributes to broad-spectrum blast resistance in rice. *Proceedings of the National Academy of Sciences, USA* 116: 17572–17577.

- Liu XY, Yang J, Qian B, Cai YC, Zou X, Zhang HF, Zheng XB, Wang P, Zhang ZG. 2018. MoYvh1 subverts rice defense through functions of ribosomal protein MoMrt4 in *Magnaporthe oryzae*. *PLoS Pathogens* 14: e1007016.
- Liu XY, Zhou QK, Guo ZQ, Liu P, Shen LB, Chai N, Qian B, Cai YC, Wang WY, Yin ZY *et al.* 2020. A self-balancing circuit centered on MoOsm1 kinase governs adaptive responses to host-derived ROS in *Magnaporthe oryzae*. *eLife* 9: e61605.
- Nurnberger T, Brunner F, Kemmerling B, Piater L. 2004. Innate immunity in plants and animals: striking similarities and obvious differences. *Immunological Reviews* 198: 249–266.
- Otte S, Barlowe C. 2002. The Erv41p-Erv46p complex: multiple export signals are required in trans for COPII-dependent transport from the ER. *EMBO Journal* 21: 6095–6104.
- Otte S, Barlowe C. 2004. Sorting signals can direct receptor-mediated export of soluble proteins into COPII vesicles. *Nature Cell Biology* 6: 1189–1194.
- Qi ZQ, Liu MX, Dong YH, Zhu Q, Li LW, Li B, Yang J, Li Y, Ru YY, Zhang HF *et al.* 2016. The syntaxin protein (MoSyn8) mediates intracellular trafficking to regulate conidiogenesis and pathogenicity of rice blast fungus. *New Phytologist* 209: 1655–1667.
- Qian B, Liu XY, Jia J, Cai YC, Chen C, Zhang HF, Zheng XB, Wang P, Zhang ZG. 2018. MoPpe1 partners with MoSap1 to mediate TOR and cell wall integrity signalling in growth and pathogenicity of the rice blast fungus *Magnaporthe oryzae*. *Environmental Microbiology* 20: 3964–3979.
- Qian B, Liu XY, Ye ZY, Zhou QK, Liu P, Yin ZY, Wang WH, Zheng XB, Zhang HF, Zhang ZG. 2020. Phosphatase-associated protein MoTip41 interacts with the phosphatase MoPpe1 to mediate crosstalk between TOR and cell wall integrity signalling during infection by the rice blast fungus *Magnaporthe oryzae*. *Environmental Microbiology* 2020: 791–809.
- Rakestraw JA, Sazinsky SL, Piatasi A, Antipov E, Wittrup KD. 2009. Directed evolution of a secretory leader for the improved expression of heterologous proteins and full-length antibodies in *Saccharomyces cerevisiae*. *Biotechnology and Bioengineering* 103: 1192–1201.
- Ron D, Walter P. 2007. Signal integration in the endoplasmic reticulum unfolded protein response. *Nature Reviews Molecular Cell Biology* 8: 519–529.
- Tabas I, Ron D. 2011. Integrating the mechanisms of apoptosis induced by endoplasmic reticulum stress. *Nature Cell Biology* 13: 184–190.
- Tang W, Ru YY, Hong L, Zhu Q, Zuo RF, Guo XX, Wang JZ, Zhang HF, Zheng XB, Wang P *et al.* 2015. System-wide characterization of bZIP transcription factor proteins involved in infection-related morphogenesis of *Magnaporthe oryzae*. *Environmental Microbiology* 17: 1377–1396.
- Travers KJ, Patil CK, Wodicka L, Lockhart DJ, Weissman JS, Walter P. 2000. Functional and genomic analyses reveal an essential coordination between the unfolded protein response and ER-associated degradation. *Cell* 101: 249–258.
- Walter P, Ron D. 2011. The unfolded protein response: from stress pathway to homeostatic regulation. *Science* 334: 1081–1086.
- Wang J, Wang F, Feng Y, Mi K, Chen Q, Shang J, Chen B. 2013. Comparative vesicle proteomics reveals selective regulation of protein expression in chestnut blight fungus by a hypovirus. *Journal of Proteomics* 78: 221–230.
- Yi M, Chi MH, Khang CH, Park SY, Kang S, Valent B, Lee YH. 2009. The ER chaperone LHS1 is involved in asexual development and rice infection by the blast fungus *Magnaporthe oryzae*. *Plant Cell* 21: 681–695.
- Yin Y, Garcia MR, Novak AJ, Saunders AM, Ank RS, Nam AS, Fisher LW. 2018. Surf4 (Erv29p) binds amino-terminal tripeptide motifs of soluble cargo proteins with different affinities, enabling prioritization of their exit from the endoplasmic reticulum. *PLoS Biology* 16: e2005140.
- Yin ZY, Feng WZ, Chen C, Xu JY, Li Y, Yang LN, Wang JZ, Liu XY, Wang WH, Gao CY *et al.* 2020. Shedding light on autophagy coordinating with cell wall integrity signaling to govern pathogenicity of *Magnaporthe oryzae*. *Autophagy* 16: 900–916.
- Zhang HF, Zheng X, Zhang ZG. 2016. The *Magnaporthe grisea* species complex and plant pathogenesis. *Molecular Plant Pathology* 17: 796–804.
- Zhang SP, Liu X, Li LW, Yu R, He JL, Zhang HF, Zheng XB, Wang P, Zhang ZG. 2017. The ArfGAP protein MoGlo3 regulates the development and pathogenicity of *Magnaporthe oryzae*. *Environmental Microbiology* 19: 3982–3996.
- Zhang SJ, Xu JR. 2014. Effectors and effector delivery in *Magnaporthe oryzae*. *PLoS Pathogens* 10: e1003826.
- Zhang SP, Yang LN, Li LW, Zhong KL, Wang WH, Liu MX, Li Y, Liu XY, Yu R, He JL *et al.* 2019. System-wide characterization of MoArf GTPase family proteins and adaptor protein MoGga1 involved in the development and pathogenicity of *Magnaporthe oryzae*. *MBio* 10: e02398–e02419.
- Zhong KL, Li X, Le XY, Kong XY, Zhang HF, Zheng XB, Wang P, Zhang ZG. 2016. MoDnm1 dynamin mediating peroxisomal and mitochondrial fission in complex with MoFis1 and MoMdv1 is important for development of functional appressorium in *Magnaporthe oryzae*. *PLoS Pathogens* 12: e1005823.

Supporting Information

Additional Supporting Information may be found online in the Supporting Information section at the end of the article.

Fig. S1 Eight sites mutation were introduced to prevent splicing by unfolded protein response.

Fig. S2 Yeast complementation assay.

Fig. S3 Gene knockout strategy and expression analyses in *Magnaporthe oryzae*.

Fig. S4 Expression profiles of *MoERV29* during various developmental stages.

Fig. S5 MoErv29 partially co-located with endoplasmic reticulum and Golgi.

Fig. S6 MoErv29 is dispensable for the secretion of cytoplasmic effectors AvrPiz-t and Avr-Pia.

Fig. S7 MoErv29 is not involved in the secretion of the apoplastic effector MoBas4.

Fig. S8 Identification of the putative cargo proteins regulated by MoErv29.

Fig. S9 The $\Delta Moerv29$ mutants are impaired in the secretion of extracellular laccase and peroxidase.

Fig. S10 The gene expression pattern of putative effectors in MoErv29 cargo spectrum through qRT-PCR analysis.

Fig. S11 MoErv29 is not involved in the secretion of cytoplasmic effector AvrPi9.

Table S1 Primers used in this study.

Table S2 The cargo spectrum of MoErv29.

Table S3 Gene ontology analysis of all putative MoErv29 cargo proteins.

Please note: Wiley Blackwell are not responsible for the content or functionality of any Supporting Information supplied by the authors. Any queries (other than missing material) should be directed to the *New Phytologist* Central Office.